NIR-to-NIR two-photon bio-imaging using very bright tailored amino-heptamethines dyes

Simon Pascal, San-Hui Chi, Alexei Grichine, Veronique Martel-Frachet, Joseph Perry, Olivier Maury, Chantal Andraud
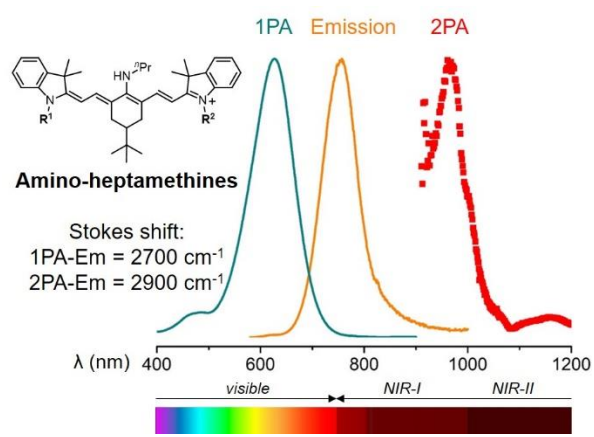
NIR-to-NIR Two-Photon Bio-Imaging Using Very Bright Tailored Amino-Heptamethines Dyes

Simon Pascal,[a,b,*] San-Hui Chi,[c] Alexei Grichine,[d] Veronique Martel-Frachet,[d,e] Joseph W. Perry,[c] Olivier Maury,[a,] Chantal Andraud[a,*]

[a] Laboratoire de Chimie, Univ. Lyon, ENS Lyon, CNRS, UMR 5182, 46 Allée d'Italie, 69364 Lyon, France. E-mail: chantal.andraud@ens-lyon.fr

[b] Centre Interdisciplinaire de Nanoscience de Marseille, Aix Marseille Univ, CNRS UMR 7325, Campus de Luminy, 13288 Marseille cedex 09, France. E-mail: simon.pascal@cnrs.fr

[c] School of Chemistry and Biochemistry, Center for Organic Photonics and Electronics
Georgia Institute of Technology, 901 Atlantic Drive NW, Atlanta, Georgia 30332-0400, United States

[d] Institute for Advanced Biosciences, University Grenoble Alpes, Inserm U1209, CNRS UMR 5309, Site Santé, Allée des Alpes, 38700, La Tronche, France

[e] EPHE, PSL Research University, 4-14 rue Ferrus, 75014, Paris, France

Abstract: Amino-heptamethines are highly conjugated cationic dyes featuring electronic absorption in the red region and strong near-infrared (NIR) fluorescence. Unlike their parent chloro-heptamethine cyanines, the substitution of the central position of their polymethine skeleton

with an amine confers them a high Stokes shift. This work reports the synthesis of amino-heptamethines and the investigation of their optical properties, including two-photon absorption in the NIR and short-wave infrared (SWIR) ranges, which has been overlooked for such chromophores so far. Their structures were tailored, introducing selected substitutuents on the indolenine moieties to modulate their hydrophobic/hydrophilic balance and investigate their potential as NIR-to-NIR two-photon probes for the bio-imaging of living cells.

1

1. Introduction

The use of near-infrared (NIR) absorbers and fluorophores is ubiquitous in various domains ranging from organic electronics [1], dye-sensitized solar cells [2], electroluminescent devices [3, 4], optical power limiting [5]-[6], photothermal therapy [7], to the development of photoacoustic [8] and fluorescence imaging bioprobes [9, 10]. Within these latter two applications, the main advantage of NIR dyes working wavelengths is their compatibility with the transparency windows of biological media, namely NIR-I and NIR-II, that spans in the ranges of 700-1000 nm and 1000-1350 nm, respectively [10-14]. Thus, excitation of the chromophore and harvest of its fluorescence in these spectral ranges provide higher contrast and deeper penetration within the tissues due to the limited auto-fluorescence and scattering, respectively. These biomedical application perspectives triggered the design of many classes of NIR-fluorophores *e.g.* charge-transfer dyes featuring very strong electron-withdrawing fragments like benzothiadiazole [15], (aza)-bodipy [16] or ytterbium complexes [17, 18].

In this context, heptamethine dyes are well-established fluorophores in the field of bio-imaging [19]. These chromophores present a symmetrical structure with a cationic charge fully delocalized (bond length alternation or BLA = 0) between two electron-donating fragments linked by an odd number of C-sp^2, seven in the case of heptamethine (Fig. 1). This particular electronic structure, called cyanine, confers to these dyes their very particular photophysical properties *i.e.* a NIR-shifted sharp absorption and emission with an extremely weak Stokes shift. Importantly, any symmetry breaking of the structure due to the solvent polarity or ion-pairing effect results in a loss of this cyanine electronic structure and the formation of a dipolar-type structure with profoundly modified photophysical properties [20-22]. The most famous dye of this family is undoubtedly the Indocyanine Green (ICG, Fig. 1), approved by the FDA for human bio-imaging and image guided surgery applications, which presents strong NIR absorption, (ε^{790} ~ 200000 M^{-1} cm^{-1}), and a fluorescence beyond 800 nm (Φ ~ 10%) resulting in a high one-photon brightness B^{790} = ε^{790}x Φ = 20000 M^{-1} cm^{-1} [23, 24]. Nevertheless, the particularly low

Stokes shift inherent to the cyanine remains an indubitable limitation to guarantee an optimized contrast when used for fluorescence imaging.
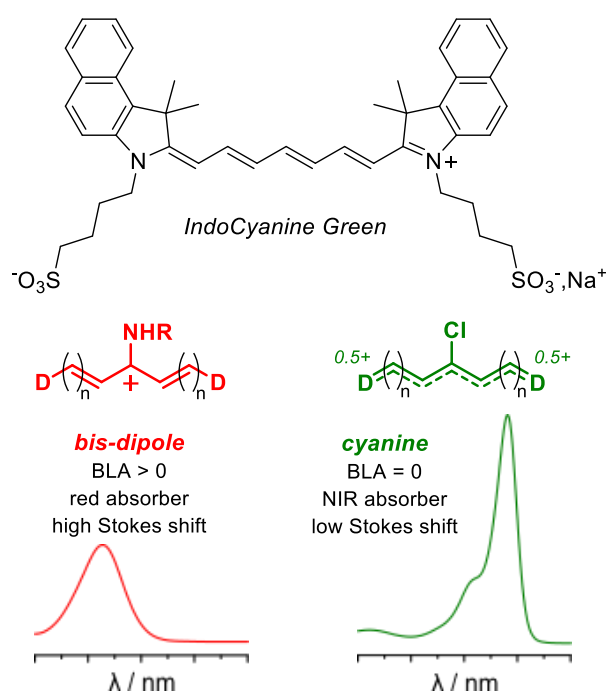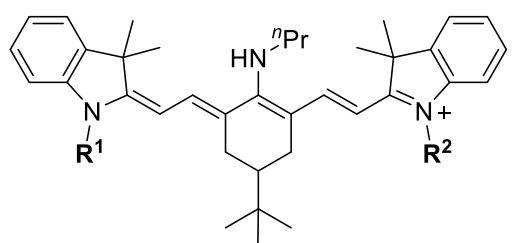

Fig. 1. Structure of ICG dye (top) and schematic representation of the bis-dipolar and cyanine electronic structures of polymethine dyes and their corresponding absorption profiles (bottom).

In 2005, the functionalization of heptamethine with a central amine function was reported as an efficient method to increase the Stokes shift [25], and amino-heptamethines thereby became popular platforms used as chemosensors [19, 26-28] for fluorophore-guided surgery [29] or microscopy and photodynamic therapy [30-34]. The large Stokes shift of this class of fluorophores is due to an intramolecular charge transfer that sensibly blue-shifts the absorption maxima while maintaining a strong emission in the deep-red region (Φ ~ 40%) [25, 35]. In fact, such hypsochromic shift appears to be inevitable since the central substitution of heptamethines with an electron-donating substituent triggers a loss of the symmetrical and highly delocalized *cyanine* electronic structure towards the establishment of a *bis-dipolar* one, featuring absorption outside of the NIR region (Fig. 1) [36, 37].

To address this issue, it is practicable to resort to a biphotonic excitation to perform NIR bio-imaging with a visible-absorbing chromophore [38-40] [41]. This strategy has been recently used to perform *in vitro* and *in vivo* NIR-to-NIR bio-imaging in the case of red-absorbing keto-polymethines, featuring a similar bis-dipolar electronic structure [42]. The subtle engineering of the indolenine functions of the dyes allowed to image mitochondria, cell membrane, or to perform angiography depending on the lipophilic/hydrophilic balance of the dye. However, the central ketone function of these polymethines limits the possibilities of bio-conjugation at this position, which is not the case of amino-heptamines, being therefore fluorophores of choice for bio-conjugation and labelling [32].

1 $R^1 = R^2 = C_6H_{13}$
2 $R^1 = R^2 = C_{12}H_{25}$
3 $R^1 = R^2 = CH_2Ph$
4 $R^1 = R^2 = (CH_2)_3SO_3^-$
5 $R^1 = C_{12}H_{25,}\ R^2 = (CH_2)_3SO_3^-$

Chart 1. Amino-heptamethine dyes investigated herein.

In the continuation of these works, we present herein the synthesis of a series of amino-heptamethines **1-5** (Chart 1) for which the hydrophilic/hydrophobic balance was modulated by tuning the substituents on the indolenine fragments (alkyl chains and/or sulfonate moieties). The two-photon absorption (2PA) properties of this class of compounds were measured for the first time, and selected candidates were tested in the context of living cells' two-photon bio-imaging in the NIR range.

4

2. Experimental

2.1. Materials and synthetic procedures

Compounds **7**, **8**, **11** [42] and amino-heptamethines **2** [43] and **3** [36] were prepared according to reported procedures. NMR spectra were recorded at room temperature on a BRUKER Avance operating at 500.1 MHz and 125.8 MHz for ^1H and ^{13}C, respectively. ^{13}C NMR signals were assigned using JMOD or HSQC experiments. Chemical shifts are listed in parts per million (δ, ppm) and are reported relative to residual solvent peaks being used as internal standard (for ^1H and ^{13}C respectively: $CDCl_3$: 7.26 and 77.2 ppm). Hydrogen atoms in equatorial or axial configuration are noted H_{eq} or H_{ax}, respectively. High resolution mass spectrometry measurements were performed at the *Centre Commun de Spectrometrie de Masse* (Villeurbanne, France).

Synthesis amino-heptamethine **1**. Chloro-heptamethine **7** (100 mg, 0.13 mmol, 1 equiv.) and distilled propylamine (0.04 mL, 0.53 mmol, 4 equiv.) were dissolved in 10 mL of anhydrous DMF and the solution was stirred for 3 hours at 85 °C. The reaction mixture was allowed to cool to room temperature and added by 20 mL of DCM and washed with water (2 x 20 mL). The organic layer was dried over Na_2SO_4 and concentrated. The crude residue was purified by flash chromatography on activated alumina (50 g Al_2O_3 mixed with 6 % H_2O) with DCM/MeOH as eluent (95:5, R_f = 0.28) to afford the product as a glossy blue solid (61 mg, 59% yield). **^1H NMR (CDCl$_3$, 500 MHz):** δ 7.72 (d, ^3J = 13 Hz, 2H, =CH), 7.20 (m, 4H, CH_{Ar}), 6.98 (t, ^3J = 7 Hz, 2H, CH_{Ar}), 6.77 (d, ^3J = 7 Hz, 2H, CH_{Ar}), 5.55 (d, ^3J = 13 Hz, 2H, =CH), 3.79 (t, ^3J = 7 Hz, 2H, N-CH_2), 3.71 (t, ^3J = 7 Hz, 4H, N-CH_2), 2.61 (d, ^2J = 11 Hz, 2H, H_{eq}), 2.02 (m, 2H, CH_2), 1.97 (dd, ^2J = 13 Hz, ^3J = 13 Hz, 2H, H_{ax}), 1.75-1.71 (m, 4H, CH_2), 1.69 (s, 6H, $C(CH_3)_2$), 1.67 (s, 6H, $C(CH_3)_2$), 1.40 (m, 4H, CH_2), 1.69-1.47 (m, 9H, CH_2 and CH), 0.98 (s, 9H, $C(CH_3)_3$), 0.91 (t, ^3J = 7 Hz, 3H, CH_3), 0.87 (t, ^3J = 7 Hz, 6H, CH_3). **$^{13}C[^1H]$ NMR (CDCl$_3$, 126 MHz):** δ 170.8 (C_{quat}), 166.3 (C_{quat}), 143.4 (C_{quat}), 140.5 (C_{quat}), 137.7 (CH), 128.0 (CH), 122.1 (CH), 122.1 (CH), 120.6

(C$_{quat}$), 107.9 (CH), 93.3 (CH), 51.8 (N-CH$_2$), 47.5 (C$_{quat}$), 44.3 (CH), 43.2 (N-CH$_2$), 32.9 (C$_{quat}$), 31.6 (CH$_2$), 29.0 (CH$_3$), 28.9 (CH$_3$), 27.3 (CH$_3$), 27.0 (CH$_2$), 26.8 (CH$_2$), 26.4 (CH$_2$), 24.2 (CH$_2$), 22.7 (CH$_2$), 14.1 (CH$_3$), 11.5 (CH$_3$). **HRMS (ESI+):** [M]$^+$ = 702.5686 (calcd for C$_{49}$H$_{72}$N$_3$: 702.5721). **UV-Vis (CH$_3$OH):** λ_{max} = 627 nm (ε_{max} = 105000 M^{-1} cm^{-1}).

Synthesis of amino-heptamethine 2. Chloro-heptamethine **8** (150 mg, 0.16 mmol, 1 equiv.) and distilled propylamine (0.05 mL, 0.65 mmol, 4 equiv.) were dissolved in 5 mL of anhydrous DMF and the solution was stirred for 3 hours at 85 °C. The reaction mixture was allowed to cool to room temperature and DMF was evaporated under reduced pressure. The residue was dissolved in 20 mL of DCM, washed with an aqueous solution of HBr 1 M (3 x 10 mL), then the organic layer was dried over Na$_2$SO$_4$ and finally concentrated. The crude residue was purified by flash chromatography on silica gel using DCM/EtOAc/MeOH (48:50:2 to 45:50:5) as eluent to afford the product as a glossy blue solid (142 mg, 92% yield). **¹H NMR (CDCl$_3$, 500 MHz):** δ 9.79 (s, 1H, NH), 7.73 (d, ^3J = 13 Hz, 2H, =CH), 7.24 (m, 4H, CH$_{Ar}$), 7.02 (t, ^3J = 8 Hz, 2H, CH$_{Ar}$), 6.80 (d, ^3J = 7 Hz, 2H, CH$_{Ar}$), 5.57 (d, ^3J = 13 Hz, 2H, =CH), 3.82 (dt, ^3J = 7 Hz, 2H, N-CH$_2$), 3.73 (t, ^3J = 7 Hz, 4H, N-CH$_2$), 2.64 (dd, ^2J = 14 Hz, ^3J = 4 Hz, 2H, H$_{eq}$), 2.08-1.96 (m, 3H, H$_{ax}$ and CH$_2$), 1.77-1.67 (m, 16H, CH$_2$ and C(CH$_3$)$_2$), 1.46-1.33 (m, 9H, CH$_2$ and CH), 1.32-1.21 (m, 28H, CH$_2$), 1.01 (s, 9H, C(CH$_3$)$_3$), 0.94 (t, ^3J = 7 Hz, 3H, CH$_3$), 0.87 (t, ^3J = 7 Hz, 6H, CH$_3$). **¹³C[¹H] NMR (CDCl$_3$, 126 MHz):** δ 170.6 (C$_{quat}$), 166.5 (C$_{quat}$), 143.4 (C$_{quat}$), 140.5 (C$_{quat}$), 137.9 (=CH), 128.0 (CH), 122.2 (CH), 122.2 (CH), 120.5 (C$_{quat}$), 107.9 (CH), 93.4 (=CH), 51.7 (N-CH$_2$), 47.6 (C$_{quat}$), 44.3 (CH), 43.3 (N-CH$_2$), 32.9 (C$_{quat}$), 32.0 (CH$_2$), 29.7 (2 CH$_2$), 29.7 (2 CH$_2$), 29.5 (CH$_2$), 29.5 (CH$_2$), 29.1 (CH$_3$), 29.0 (CH$_3$), 27.4 (CH$_2$), 27.3 (CH$_3$), 26.8 (CH$_2$), 26.5 (CH$_2$), 24.3 (CH$_2$), 22.8 (CH$_2$), 14.3 (CH$_3$), 11.5 (CH$_3$). **HRMS (ESI+):** [M]$^+$ = 870.7582 (calcd for C$_{61}$H$_{96}$N$_3$: 870.7599). **UV-Vis (CH$_3$OH):** λ_{max} = 628 nm (ε_{max} = 97000 M^{-1} cm^{-1}).

*Synthesis of amino-heptamethine **5**.* Chloro-heptamethine **11** (90 mg, 0.11 mmol, 1 equiv.) and distilled propylamine (0.04 mL, 0.45 mmol, 4 equiv.) were dissolved in 3 mL of anhydrous DMF and the solution was stirred for 3 hours at 80 °C. The reaction mixture was allowed to cool to room temperature and DMF was evaporated under reduced pressure. The residue was dissolved in 20 mL of DCM, washed with an aqueous solution of HBr 1 M, then the organic layer was dried over Na_2SO_4 and finally concentrated. The crude was purified by flash chromatography on silica gel using DCM/ MeOH (90:10, R_f = 0.65) as eluent to afford the product as a glossy blue solid (75 mg, 81% yield). **^{1}H NMR (CDCl$_3$, 500 MHz):** δ 10.15 (s, 1H, NH), 8.08 (d, ^3J = 13 Hz, 1H, =CH), 7.29-7.19 (m, 5H, =CH and CH$_{Ar}$), 7.01 (m, 2H, CH$_{Ar}$), 6.87 (d, ^3J = 8 Hz, 1H, CH$_{Ar}$), 6.78 (d, ^3J = 8 Hz, 1H, CH$_{Ar}$), 5.44 (d, ^3J = 13 Hz, 1H, =CH), 5.27 (d, ^3J = 13 Hz, 1H, =CH), 5.44 (d, ^2J = 13 Hz, 1H, CH$_2$), 4.48 (m, 1H, CH$_2$), 4.41 (m, 1H, CH$_2$), 3.88 (m, 1H, CH$_2$), 3.76 (m, 1H, CH$_2$), 3.72 (m, 2H, CH$_2$), 3.12 (m, 2H, CH$_2$), 2.79 (d, ^2J = 15 Hz, 1H, H$_{eq}$), 2.61 (d, ^2J = 15 Hz, 1H, H$_{eq}$), 2.24 (m, 2H, CH$_2$), 2.19 (dd, ^2J = 14 Hz, ^3J = 14 Hz, 1H, H$_{ax}$), 2.07 (m, 2H, CH$_2$), 1.92 (dd, ^2J = 14 Hz, ^3J = 14 Hz, 1H, H$_{ax}$), 1.74 (m, 4H, CH$_2$), 1.57 (s, 3H, C(CH$_3$)$_2$), 1.53 (s, 3H, C(CH$_3$)$_2$), 1.45-1.39 (m, 3H, CH and CH$_2$), 1.38 (s, 3H, C(CH$_3$)$_2$), 1.37 (s, 3H, C(CH$_3$)$_2$), 1.31-1.23 (m, 14H, CH$_2$), 1.03 (s, 9H, C(CH$_3$)$_3$), 0.95 (t, ^3J = 7 Hz, 3H, CH$_3$), 0.88 (t, ^3J = 7 Hz, 3H, CH$_3$). **^{13}C[^{1}H] NMR (CDCl$_3$, 126 MHz):** δ 172.1 (C$_{quat}$), 164.7 (C$_{quat}$), 163.5 (C$_{quat}$), 144.7 (C$_{quat}$), 143.5 (C$_{quat}$), 139.7 (C$_{quat}$), 138.3 (C$_{quat}$), 136.6 (CH), 133.0 (CH), 128.3 (CH), 128.1 (CH), 122.6 (C$_{quat}$), 122.4 (CH), 122.1 (2 CH), 122.0 (CH), 118.7 (C$_{quat}$), 108.1 (CH), 107.7 (CH), 91.7 (CH), 51.8 (CH$_2$), 48.4 (C$_{quat}$), 48.2 (CH$_2$), 47.0 (C$_{quat}$), 45.0 (CH$_2$), 43.5 (CH), 43.1 (CH$_2$), 32.6 (C$_{quat}$), 32.0 (CH$_2$), 29.8 (2 CH$_2$), 29.7 (2 CH$_2$), 29.5 (CH$_2$), 29.5 (2 CH$_3$), 29.4 (CH$_2$), 29.3 (CH$_3$), 28.8 (CH$_3$), 27.9 (CH$_2$), 27.5 (CH$_3$), 27.4 (CH$_2$), 27.1 (CH$_2$), 26.4 (CH$_2$), 23.3 (CH$_2$), 22.8 (CH$_2$), 22.7 (CH$_2$), 14.3 (CH$_3$), 11.6 (CH$_3$). **HRMS (ESI+):** [M+H]$^+$ = 824.5727 (calcd for C$_{52}$H$_{78}$N$_3$O$_3$S: 824.5758). **UV-Vis (MeOH):** λ_{max} = 624 nm (ε_{max} = 94000 M^{-1} cm^{-1}).

2.2. **Linear absorption and luminescence.**

Absorption spectra were recorded on a JASCO V-650 spectrophotometer in diluted solution (*ca.* 10^{-6} M) using spectrophotometric grade solvents. Molar extinction coefficients (ε) were precisely determined at least two times. Emission spectra were measured using a Horiba-Jobin-Yvon Fluorolog-3 iHR320 fluorimeter. Fluorescence quantum yields Q were measured in diluted solutions with an absorbance lower than 0.1 using the following equation $Q_x/Q_r = [A_r(\lambda)/A_x(\lambda)][n_x^2/n_r^2][D_x/D_r]$ were A is the absorbance at the excitation wavelength (λ), n the refractive index and D the integrated luminescence intensity. "r" and "x" stand for reference and sample. The fluorescence quantum yields were measured relative to Crystal Violet in methanol (Φ = 0.55). Excitation of reference and sample compounds was performed at the same wavelength. Short luminescence decay was monitored with the TC-SPC Horiba apparatus using Ludox in distilled water to determine the instrumental response function used for deconvolution. Excitation was performed using NanoLEDs, with model 570 (573 nm; 1.5 ns). The deconvolution was performed using the DAS6 fluorescence-decay analysis software. The photostability measurement were conducted with compound **1** dissoved in methanol (*ca.* 2.5×10^{-6} M) and under continuous stirring. Calibration of the fluorimeter irradiation was measured with a ThorLab power-meter (Fig. S9). The slits were fixed at 8 nm to avoid detector saturation and, consequently, the incident power was fixed at P_{inc} = 2.17 mW.

2.3. Two-photon absorption

A solution of compound **1** was prepared in spectroscopic grade methanol (Sigma Aldrich) with a concentration of ~1.3 mM for ND-2PA and open aperture z-scan measurements. The two-photon absorption (2PA) spectra were mapped with femtosecond-pulsed ND-2PA spectrometer [44, 45], and the 2PA absorption cross sections, σ in GM, were confirmed with femtosecond-pulsed open aperture z-scan techniques. The optical pathlength of the sample cuvette is 2 mm for ND-2PA and 1mm for z-scan. For ND-2PA measurements, excitation

wavelengths of 925, 1300, and 1550 nm and a white light continuum (WLC) probe ranging from ~850-1600 nm were selected to acquire the ND-2PA spectra from ~900-1500 nm. The two-photon wavelengths are obtained with Eq. (1).

$$\lambda_{ND2PA} = \frac{2}{(\lambda_{pump})^{-1} + (\lambda_{probe})^{-1}} \quad (1)$$

where λ_{pump} and λ_{probe} are the excitation and probing wavelengths. By definition, the ND-2PA measured two-photon cross section (δ_{ND}) should be 2× larger than the z-scan measured degenerated two-photon cross section (δ_D).

For z-scan measurements, a near Gaussian beam at 900, 1000, and 1200 nm with $M^2 <$ 1.1, $\omega(HW_{1/e2}) \sim 60$ µm, and $\tau p(HW_{1/e}) \sim 75$ fs was used. The excitation irradiance ranges from 60 – 400 GW/cm^2. The optical pathlength of sample cuvettes is 1 mm.

2.4. Cell culture and staining

A human embryonic kidney cancer cell line (HEK-293, ATCC no. CRL-1573) was used. HEK-293 cells were cultured in RPMI 1640 supplemented with 10% fetal calf serum at 37 °C in a humidified atmosphere with 5% CO_2. For imaging experiments, cells were seeded on a LabTek I chambered cover glass (Thermo Scientific Nunc, Rochester, USA) at low cell density in a complete culture medium and grown to semi-confluence 24 h. The medium was rinsed and replaced by PBS solution before experiments.
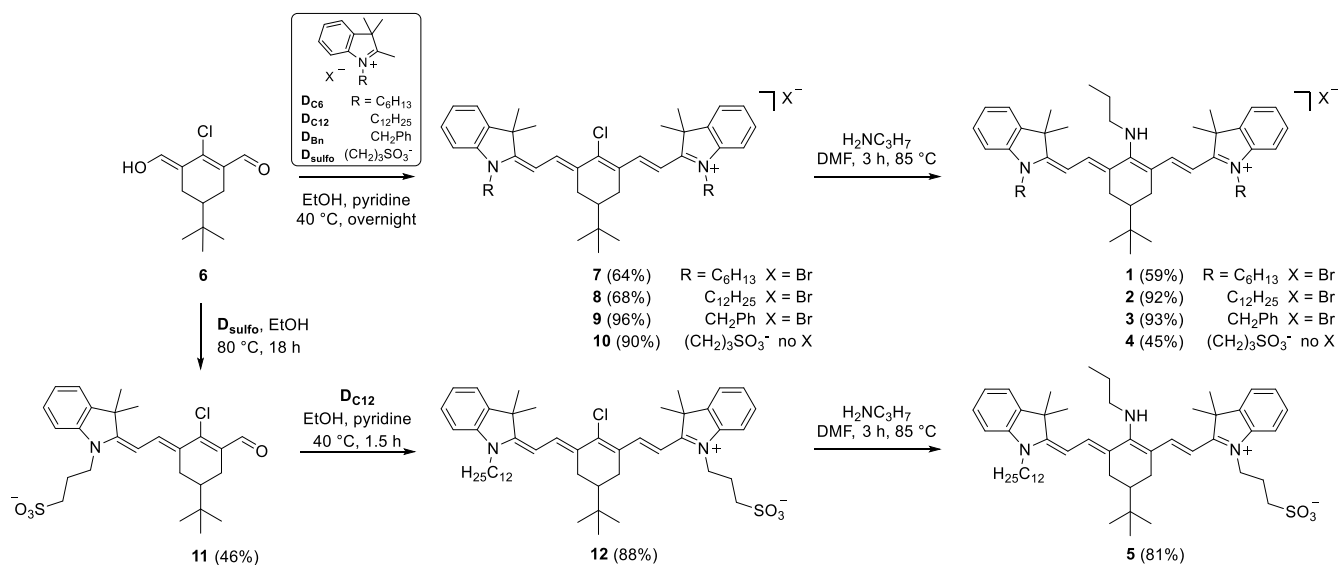
2.5. Two-photon microscopy

The two-photon experiments were performed using a LSM710 NLO – ConfoCor3 (Carl Zeiss) confocal laser scanning microscope based on the inverted motorized stand (AxioObserver) in descanned detection mode with the open pinhole. The C-Apochromat 40x/1.2 water immersion objective was used. The two-photon excitation was provided by Ti:Sa femtosecond laser (Chameleon, Ultra II, Coherent) tuned to 900 nm, featuring 140 fs pulses at 80 MHz. Cells were kept at 37 °C and 5% CO_2 throughout acquisitions due to the on-stage

incubator. Depending on the probe intensity, either spectral PMT detector 'quasar' was used in 700-758 nm range or an APD detector of the ConfoCor3 unit with the bandpass filter 655-710 nm.

3. Results and Discussion

The synthesis of amino-heptamethines **1-5** is presented in Scheme 1 and consists in the Knoevenagel condensation of two equivalents of indolenium salt on the bis-aldehyde **6** leading to the formation of chloro-heptamethines **7-10**. Then the nucleophilic substitution is performed with an excess of distilled propylamine at 85 °C in *N,N*-dimethylformamide and the target compounds are obtained with moderate to high yields (45-93%) after purification by column chromatography. The access to the dissymmetrical amino-heptamethine **5** requires the synthesis of the merocyanine intermediate **11** featuring a free aldehyde function which undergoes a second condensation with one additional equivalent of indolenium salt giving the heptamethine **12**. This latter is finally substituted in the presence of propylamine, and the amphiphilic compound **5** is isolated as a glossy blue solid in 81% yield following simple flash column chromatography.

Scheme 1. Synthesis of amino-heptamethines **1-5**.

The photophysical properties of the series were measured in methanol solutions at room temperature (Fig. 2 and Table 1). All the amino-heptamethines present a broad and quasi-Gaussian absorption with maxima centered around 617-628 nm, thus remaining poorly influenced by the different substituents on the indolenine nitrogen atoms. However, while the molar extinction coefficients are *ca*. 100000 $M^{-1} cm^{-1}$ for the lipophilic and amphiphilic derivatives, it drops to 68000 $M^{-1} cm^{-1}$ in the case of hydrophilic compound **4**. The emission maxima are all measured around 758 nm, affording Stokes shifts Δ_{SS} ~ 2700-3000 cm^{-1}, and with cut-off wavelengths reaching 850 nm. The fluorescence is characterized by average quantum yields and lifetimes *ca*. 20% and 0.8 ns, respectively leading to a very high brightness in methanol in this spectral range of *ca.* 20000 $M^{-1} cm^{-1}$. It is noteworthy that, in water, the hydrosoluble compound **4** presents an emission band in the NIR at 764 nm with a reasonable 6% quantum yield making it suitable for bio-imaging experiments (B_{H2O} = 2940 $M^{-1} cm^{-1}$) [32].
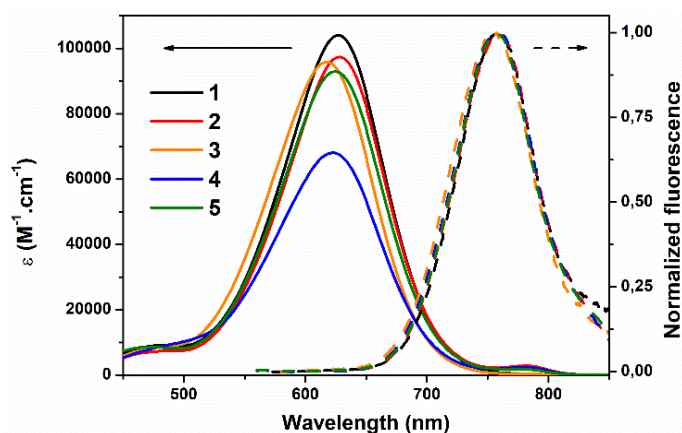

Fig. 2. Electronic absorption (plain lines) and normalized fluorescence (dashed lines) spectra of compounds **1-5** in methanol.

Table 1. Photophysical properties in methanol.

Dye	λ_{abs} (nm)	ε (M^{-1} cm^{-1})	λ_{em} (nm)	Δ_{SS} (cm^{-1})	$\Phi^{[a]}$ (%)	τ (ns)$^{[b]}$
1	627	105000	757	2700	21	0.9
2	628	97000	759	2800	21	0.9
3	617	96000	759	3000	20	0.9
4	623	68000	759	2900	18	0.7
5	624	94000	757	2800	19	0.8

[a] Reference: Crystal Violet (methanol, Φ = 55%). [b] NanoLED excitation at 573 nm.

To gain further insight into the spectroscopy of this series, we conducted fluorescence measurements of amino-heptamethine **3** and chloro-heptamethine **9** at 77 K in an organic glass (methanol-ethanol, 1:4). Absorption, emission, and excitation spectra are described in Fig. 3, and the photophysical data, including excitation and emission full width at half-maximum (FWHM) and Stokes shift (Δ_{SS}), are compiled in Table 2. Importantly, the low-temperature emission of compound **3** is strongly blue-shifted to 657 nm, with $\Delta\lambda_{em}$ = 100 nm (2010 cm^{-1}) compared to the fluorescence recorded at 298 K. This variation results in a significant decrease of the Stokes shift of **3** (Δ_{SS}) from 2714 to 805 cm^{-1}, the value being still lower than that of the chloro-heptamethine **9** (Δ_{SS} = 313 cm^{-1} at 298 K). In addition, both the fluorescence and the corresponding excitation spectra are noticeably sharpened compared to the room temperature ones (see Table 2). The behavior of **3** is then profoundly modified at low temperature and becomes reminiscent of a cyanine electronic structure, as illustrated by the comparison with compound **9** absorption and fluorescence spectra recorded at 298 and 77 K (Fig. 3, bottom). It is worth noting that the temperature effect is more pronounced in the emission of **3** than in absorption. It is well known that the low temperature and the more rigid glassy solid matrix strongly reduce the molecular motions during the excited state relaxation process and avoid solvent reorganization around the excited chromophore. This effect is stronger in the case of **3,** featuring a bis-dipole electronic configuration with a V-shape charge transfer type transition. As

already observed [46], the relaxation process leading to the stabilization of the cationic charge by the nitrogen lone pair of the central amino-group is no longer occurring at 77K, leading to a more delocalized excited-state structure similar to that of **9**. This temperature effect again illustrates the very high polarizability of the π-conjugated system of polymethine dyes where minor perturbations can induce profound modifications of the photophysical properties.
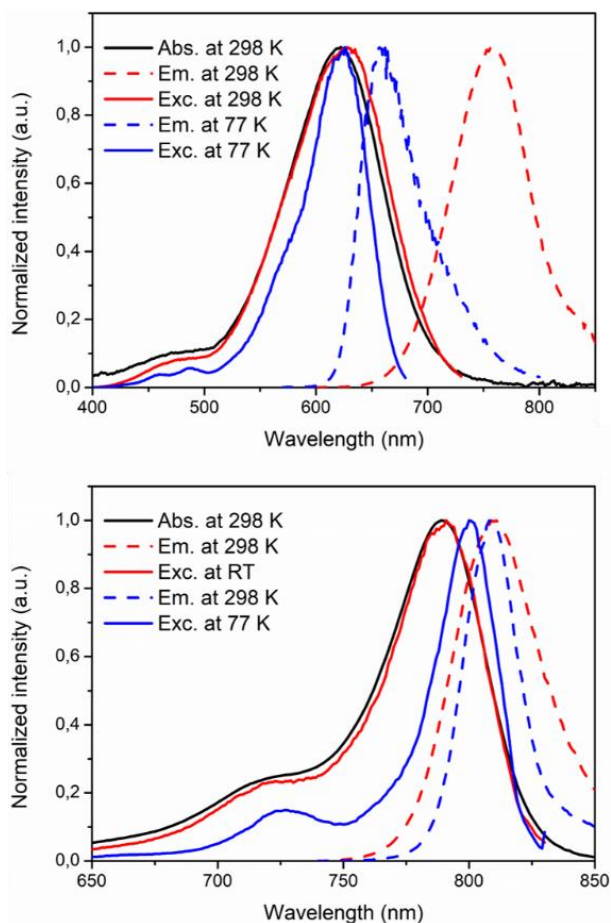

Fig. 3. Normalized absorption (Abs., black curves), emission (Em.), and excitation (Exc.) spectra were recorded at 298 K (red curves) or 77 K (blue curves) for amino-heptamethines **3** (top) and chloro-heptamethines **9** (bottom) in an ethanol/methanol mixture (1:4).

Table 2. Photophysical data for heptamethines **3** and **9** at 298 and 77 K in an ethanol/methanol mixture (1:4).

Dye	T (K)	λ^{abs} (nm)	λ^{exc} (nm)	λ^{em} (nm)	FWHM^{exc} (cm^{-1})	FWHM^{em} (cm^{-1})	Δ_{SS} (cm^{-1})
3	298	622	628	757	2790	1420	2700
	77	-	624	657	1710	1370	805
9	298	790	790	810	711	623	310
	77	-	800	808	455	383	120

Since the *meso* substitution of polymethines with electron-rich groups can impact its photostability due to possible reactions with singlet oxygen [47-49], the photobleaching of amino-heptamethine dye **1** was investigated in methanol (A = 0.26) and its emission was monitored upon irradiation at 630 nm (Fig. S10). A linear decrease of the emission intensity was observed with a very small slope. After 2.5 hours of irradiation, the photobleaching was measured at 6.5%. The absorption spectra were recorded, indicating a variation of optical density at 630 nm after irradiation (ΔA = 0.013), which corresponds to a 5% decrease and confirms the photoluminescence measurement. Such moderate bleaching under irradiation in aerated solution is partially attributed to the cyclohexyl ring appending the polymethine chain that improves its resistance compared to parent streptocyanines, nevertheless it must be kept in mind that the potential reactions with singlet oxygen may be favoured in aqueous medium [47, 49].

To be considered a potential NIR-to-NIR bio-probe for two-photon microscopy, a chromophore must present significant two-photon absorption to complement the above-mentioned fluorescence properties. To that end, the non-degenerate two-photon absorption (ND-2PA) spectrum and open-aperture z-scan degenerated 2PA cross sections were measured in methanol for compound **1** and are shown in Fig. 4. The 2PA maximum is found at 970 nm with a cross-section δ ~ 940 GM and therefore **1** presents a significant two-photon brightness,

noted $B^{(2)}$ in the NIR (at 970 nm, $B^{(2)} = \delta^{790} \times \Phi = 940 \times 0.21 = 197$ GM in methanol). This band is blue-shifted compared to the lower-energy 1P-transition, which reveals that the bent quasi-C_{2v} symmetry of the molecules confers a quadrupolar-like behaviors towards 2PA, as already noticed for keto-heptamethines [42]. The residual dipolar character of the dye gives an additional weak 2PA absorption in the SWIR (NIR-II) range at *ca.* 1210 nm, with $\delta \sim 90$ GM and a corresponding $B^{(2)}$ value of 19 GM at 1210 nm.
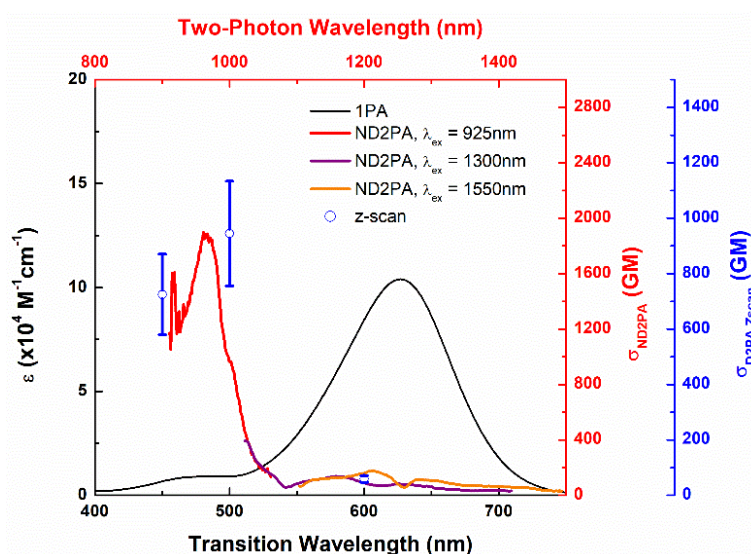

Fig. 4. 1PA and ND-2PA spectra of **1** in methanol. The black line (—) indicates the one-photon absorption spectrum; the ND-2PA spectrum is represented by red, purple, and orange lines, corresponding to different excitation wavelengths (λ_{ex}, as noted in the legend); the blue open circle (○) is the z-scan measured 2PA cross sections (excitation wavelengths are $\lambda = 1350$ and 1500 nm). It should be noted that the dips in ND-2PA spectrum at transition wavelength 600-650 nm are due to the scattering of excitation wavelengths of 1300 and 1550 nm.

Human embryonic kidney (HEK-293) cells were imaged with various amino-heptamethine dyes presenting different substituents at the indole position to study the influence of the hydrophilicity/hydrophobicity on the internalization and localization processes. Three dyes were tested: the hydrophobic chromophores **1** and **2** featuring two long alkyl chains, and the amphiphilic unsymmetrical chromophore **5** bearing an anionic sulfonate fragment and a

15

lipophilic chain at its two extremities. As expected, the dyes **1-2** are poorly soluble in aqueous medium while **5** is highly water-soluble. Thus, the cell staining was performed with stock solutions of dyes in DMSO (**1**, **2**) or water (**5**), resulting in an overall chromophore concentration in the medium of *ca.* 1–2 x 10^{-5} M and DMSO or water addition of less than 1%, known to induce very moderate cytotoxic effects. The imaging experiments were carried out after 30 min of incubation without rinsing. In all cases, NIR-to-NIR two-photon imaging experiments were performed with laser excitation at 900 nm and detection in the 700-758 nm range with the PMT detector. In case of a very faint signal (compound **5**, short incubation time), a more sensitive avalanche photodiode detector (APD) was used in the far-red/NIR spectral detection range 655-710 nm. Representative images are reported in Fig. 5.

The hydrophobic compound (**1**) presents the cytosolic localization pattern with the preferential accumulation in the perinuclear filamentous structures, probably being mitochondria. It also strongly stains punctuate organelles close to the plasma membrane, which perfectly co-localize with the lipid droplets visible in DIC image. In some cells we noted a moderate homogenous staining of the nuclei, without preferential accumulation in the nucleoli. The most lipophilic dye (**2**) is also spontaneously and rapidly internalized in the living cells, where it diffusely accumulates inside the cytosol and much less in the nucleus. Additionally, strongly stained vesicular structures can be observed throughout the cytosol, without clear co-localization with the structures visible in transmitted light. Finally, the amphiphilic compound (**5**) is only partly internalized in living cells after a short (0.5 - 1 h) period of incubation. It mostly stays in the extracellular medium, and consequently, the image contrast is very poor (Fig. 5, third row). However, a longer (24 h) incubation of cells in these conditions results in a strong accumulation of the compound **5** in the cytoplasmic organelles and structures, which seem to be the nuclear membrane, the endoplasmic reticulum, and probably mitochondria (Fig. 5, fourth row). Neither intense vesicular structures nor nuclear staining is noted.
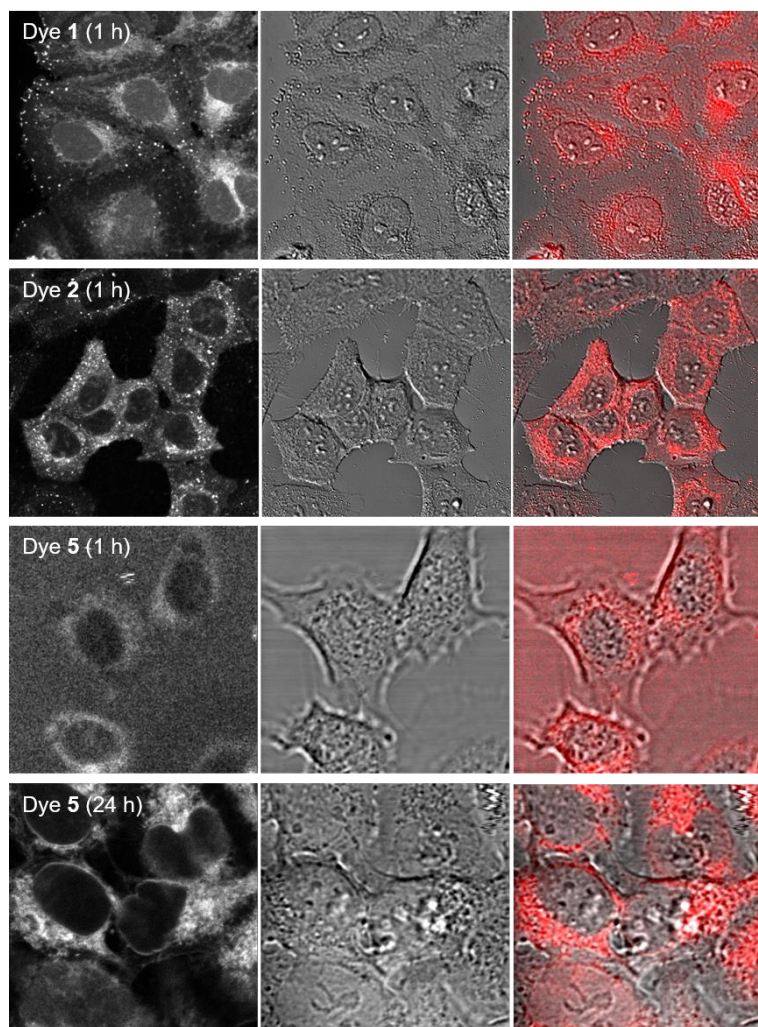
Fig. 5. Two photon excited fluorescence microscopy (left), transmission (center), and merged (right) images of HEK-293 cells after their 1 h incubation with **1** (first row), **2** (second row) **5** (third row) and 24 h incubation with **5** (fourth row). 2P excitation was performed at 900 nm.

The dye fluorescence in the culture medium is much lower after the long-term incubation, in agreement with the observed sequestration of the probe by the cells. Importantly, the cell viability and proliferation are not impaired by the presence of the dye over 24 hours. The cell entry mode and the organelle staining thus strongly depend on the overall probe hydrophobicity and its molecular distribution, allowing the fine-tuning of the accumulation pattern. This strategy, combined with the NIR-to-NIR imaging and the very low probe toxicity, opens the way to follow the subcellular organelle distribution deep inside the tissues or the multicellular organoids, which is often related to the metabolic or differentiation status of cells.

4. Conclusion

Beyond providing protocols to synthesize amino-heptamethine dyes featuring lipophilic and hydrophilic substituents on the indolenine moieties, this study illustrated their potential for NIR-to-NIR two-photon bio-imaging with excitation and emission occuring in the 750-900 nm range. The staining of living cells highlighted a prompt internalization of the hydrophobic dyes, with localization in cytosol and small organelles such as mitochondria, while the amphiphilic derivative requires longer incubation time and tends to moreover stain the nuclear membrane and the endoplasmic reticulum. A main perspective of this work would consist in the engineering of the central substituent using arylamines to tune and increase the nonlinear absorption *ca.* 1200 nm, paving the way to SWIR-to-NIR bio-imaging.

Appendix A. Supplementary data

Supplementary data to this article can be found online at:

https://www.sciencedirect.com/science/article/abs/pii/S0143720822002911?via%3Dihub.

References

[1] Qian G, Wang ZY. Near-Infrared Organic Compounds and Emerging Applications. Chem Asian J. 2010;5(5):1006-29.
[2] Brogdon P, Cheema H, Delcamp JH. Near-Infrared-Absorbing Metal-Free Organic, Porphyrin, and Phthalocyanine Sensitizers for Panchromatic Dye-Sensitized Solar Cells. ChemSusChem. 2018;11(1):86-103.
[3] Seo S, Pascal S, Park C, Shin K, Yang X, Maury O, et al. NIR electrochemical fluorescence switching from polymethine dyes. Chem Sci. 2014;5(4):1538-44.
[4] Lim H, Seo S, Pascal S, Bellier Q, Rigaut S, Park C, et al. NIR Electrofluorochromic Properties of Aza-Boron-dipyrromethene Dyes. Sci Rep. 2016;6:18867.

[5] Pascal S, Bellier Q, David S, Bouit P-A, Chi S-H, Makarov NS, et al. Unraveling the Two-Photon and Excited-State Absorptions of Aza-BODIPY Dyes for Optical Power Limiting in the SWIR Band. J Phys Chem C. 2019;123(38):23661-73.

[6] Pascal S, David S, Andraud C, Maury O. Near-infrared dyes for two-photon absorption in the short-wavelength infrared: strategies towards optical power limiting. Chem Soc Rev. 2021;50(11):6613-58.

[7] Zhu H, Cheng P, Chen P, Pu K. Recent progress in the development of near-infrared organic photothermal and photodynamic nanotherapeutics. Biomater Sci. 2018;6(4):746-65.

[8] Miao Q, Pu K. Organic Semiconducting Agents for Deep-Tissue Molecular Imaging: Second Near-Infrared Fluorescence, Self-Luminescence, and Photoacoustics. Adv Mater. 2018:1801778.

[9] Hong G, Antaris AL, Dai H. Near-infrared fluorophores for biomedical imaging. Nature Biomed Eng. 2017;1:0010.

[10] Kenry, Duan Y, Liu B. Recent Advances of Optical Imaging in the Second Near-Infrared Window. Adv Mater. 2018:1802394.

[11] Hemmer E, Benayas A, Légaré F, Vetrone F. Exploiting the biological windows: current perspectives on fluorescent bioprobes emitting above 1000 nm. Nanoscale Horiz. 2016;1(3):168-84.

[12] Jiang Y, Pu K. Molecular Fluorescence and Photoacoustic Imaging in the Second Near-Infrared Optical Window Using Organic Contrast Agents. Adv Biosys. 2018;2(5):1700262.

[13] Ding F, Zhan Y, Lu X, Sun Y. Recent advances in near-infrared II fluorophores for multifunctional biomedical imaging. Chem Sci. 2018;9(19):4370-80.

[14] Lei Z, Zhang F. Molecular Engineering of NIR-II Fluorophores for Improved Biomedical Detection. Angewandte Chemie International Edition. 2021;60(30):16294-308.

[15] Zhu S, Herraiz S, Yue J, Zhang M, Wan H, Yang Q, et al. 3D NIR-II Molecular Imaging Distinguishes Targeted Organs with High-Performance NIR-II Bioconjugates. Adv Mater. 2018;30(13):e1705799.

[16] Shi Z, Han X, Hu W, Bai H, Peng B, Ji L, et al. Bioapplications of small molecule Aza-BODIPY: from rational structural design to in vivo investigations. Chemical Society Reviews. 2020;49(21):7533-67.

[17] Hamon N, Roux A, Beyler M, Mulatier JC, Andraud C, Nguyen C, et al. Pyclen-Based Ln(III) Complexes as Highly Luminescent Bioprobes for In Vitro and In Vivo One- and Two-Photon Bioimaging Applications. J Am Chem Soc. 2020;142(22):10184-97.

[18] Jin G-Q, Ning Y, Geng J-X, Jiang Z-F, Wang Y, Zhang J-L. Joining the journey to near infrared (NIR) imaging: the emerging role of lanthanides in the designing of molecular probes. Inorganic Chemistry Frontiers. 2020;7(2):289-99.

[19] Sun W, Guo S, Hu C, Fan J, Peng X. Recent Development of Chemosensors Based on Cyanine Platforms. Chem Rev. 2016;116(14):7768-817.

[20] Eskandari M, Roldao JC, Cerezo J, Milián-Medina B, Gierschner J. Counterion-Mediated Crossing of the Cyanine Limit in Crystals and Fluid Solution: Bond Length Alternation and Spectral Broadening Unveiled by Quantum Chemistry. Journal of the American Chemical Society. 2020;142(6):2835-43.

[21] Bouit P-A, Aronica C, Toupet L, Le Guennic B, Andraud C, Maury O. Continuous Symmetry Breaking Induced by Ion Pairing Effect in Heptamethine Cyanine Dyes: Beyond the Cyanine Limit. Journal of the American Chemical Society. 2010;132(12):4328-35.

[22] Pascal S, Chi S-H, Perry JW, Andraud C, Maury O. Impacts of Ion-Pairing Effects on Linear and Nonlinear Photophysical Properties of Polymethines Dyes. ChemPhysChem. 2020;21(23):2536-42.

[23] Rurack K, Spieles M. Fluorescence Quantum Yields of a Series of Red and Near-Infrared Dyes Emitting at 600−1000 nm. Anal Chem. 2011;83(4):1232-42.

[24] Cosco ED, Lim I, Sletten EM. Photophysical Properties of Indocyanine Green in the Shortwave Infrared Region. ChemPhotoChem. 2021;5(8):727-34.

[25] Peng X, Song F, Lu E, Wang Y, Zhou W, Fan J, et al. Heptamethine Cyanine Dyes with a Large Stokes Shift and Strong Fluorescence: A Paradigm for Excited-State Intramolecular Charge Transfer. Journal of the American Chemical Society. 2005;127(12):4170-1.

[26] Zhang C, Gao R, Zhang L, Liu C, Yang Z, Zhao S. Design and Synthesis of a Ratiometric Photoacoustic Probe for In Situ Imaging of Zinc Ions in Deep Tissue In Vivo. Anal Chem. 2020;92(9):6382-90.

[27] Zhang C, Qiu Z, Zhang L, Pang Q, Yang Z, Qin J-K, et al. Design and synthesis of a ratiometric photoacoustic imaging probe activated by selenol for visual monitoring of pathological progression of autoimmune hepatitis. Chem Sci. 2021;12(13):4883-8.

[28] Lucero MY, East AK, Reinhardt CJ, Sedgwick AC, Su S, Lee MC, et al. Development of NIR-II Photoacoustic Probes Tailored for Deep-Tissue Sensing of Nitric Oxide. Journal of the American Chemical Society. 2021;143(18):7196-202.

[29] Njiojob CN, Owens EA, Narayana L, Hyun H, Choi HS, Henary M. Tailored Near-Infrared Contrast Agents for Image Guided Surgery. Journal of Medicinal Chemistry. 2015;58(6):2845-54.

[30] Yen SK, Jańczewski D, Lakshmi JL, Dolmanan SB, Tripathy S, Ho VHB, et al. Design and Synthesis of Polymer-Functionalized NIR Fluorescent Dyes–Magnetic Nanoparticles for Bioimaging. ACS Nano. 2013;7(8):6796-805.

[31] Shen Z, Prasai B, Nakamura Y, Kobayashi H, Jackson MS, McCarley RL. A Near-Infrared, Wavelength-Shiftable, Turn-on Fluorescent Probe for the Detection and Imaging of Cancer Tumor Cells. ACS Chem Biol. 2017;12(4):1121-32.

[32] Wang T-C, Cochet F, Facchini FA, Zaffaroni L, Serba C, Pascal S, et al. Synthesis of the New Cyanine-Labeled Bacterial Lipooligosaccharides for Intracellular Imaging and in Vitro Microscopy Studies. Bioconjugate Chem. 2019;30(6):1649-57.

[33] Meng X, Yang Y, Zhou L, Zhang l, Lv Y, Li S, et al. Dual-Responsive Molecular Probe for Tumor Targeted Imaging and Photodynamic Therapy. Theranostics. 2017;7(7):1781-94.

[34] Jiao L, Song F, Cui J, Peng X. A near-infrared heptamethine aminocyanine dye with a long-lived excited triplet state for photodynamic therapy. Chemical Communications. 2018;54(66):9198-201.

[35] Zhang J, Moemeni M, Yang C, Liang F, Peng W-T, Levine BG, et al. General strategy for tuning the Stokes shifts of near infrared cyanine dyes. Journal of Materials Chemistry C. 2020;8(47):16769-73.

[36] Pascal S, Haefele A, Monnereau C, Charaf-Eddin A, Jacquemin D, Le Guennic B, et al. Expanding the Polymethine Paradigm: Evidence for the Contribution of a Bis-Dipolar Electronic Structure. J Phys Chem A. 2014;118(23):4038-47.

[37] Pascal S, Haefele A, Monnereau C, Charaf-Eddin A, Jacquemin D, Le Guennic B, et al. On the versatility of electronic structures in polymethine dyes. Proc SPIE. 2014;9253A:1-11.

[38] Two-photon fluorescent probes for bioimaging. Eur J Org Chem. 2012;2012:3199.

[39] Kim D, Ryu HG, Ahn KH. Recent development of two-photon fluorescent probes for bioimaging. Organic & Biomolecular Chemistry. 2014;12(26):4550-66.

[40] Hong-Wen L, Yongchao L, Peng W, Xiao-Bing Z. Molecular engineering of two-photon fluorescent probes for bioimaging applications. Methods Appl Fluoresc. 2017;5(1):012003.

[41] Yao S, Belfield KD. Two-Photon Fluorescent Probes for Bioimaging. European Journal of Organic Chemistry. 2012;2012(17):3199-217.

[42] Pascal S, Denis-Quanquin S, Appaix F, Duperray A, Grichine A, Le Guennic B, et al. Keto-polymethines: a versatile class of dyes with outstanding spectroscopic properties for in cellulo and in vivo two-photon microscopy imaging. Chem Sci. 2017;8(1):381-94.

[43] Grichine A, Haefele A, Pascal S, Duperray A, Michel R, Andraud C, et al. Millisecond lifetime imaging with a europium complex using a commercial confocal microscope under one or two-photon excitation. Chem Sci. 2014;5(9):3475-85.

[44] Negres RA, Hales JM, Hagan DJ, Van Stryland EW. Experiment and analysis of two-photon absorption spectroscopy using a white-light continuum probe. Ieee J Quantum Elect. 2002;38(9):1205-16.

[45] Getmanenko YA, Hales JM, Balu M, Fu J, Zojer E, Kwon O, et al. Characterisation of a dipolar chromophore with third-harmonic generation applications in the near-IR. J Mater Chem. 2012;22(10):4371-82.

[46] Sissa C, Painelli A, Terenziani F, Trotta M, Ragni R. About the origin of the large Stokes shift in aminoalkyl substituted heptamethine cyanine dyes. Phys Chem Chem Phys. 2019;22(1):129-35.

[47] Samanta A, Vendrell M, Das R, Chang Y-T. Development of photostable near-infrared cyanine dyes. Chemical Communications. 2010;46(39):7406-8.

[48] Nani RR, Kelley JA, Ivanic J, Schnermann MJ. Reactive species involved in the regioselective photooxidation of heptamethine cyanines. Chem Sci. 2015;6(11):6556-63.

[49] Štacková L, Muchová E, Russo M, Slavíček P, Štacko P, Klán P. Deciphering the Structure–Property Relations in Substituted Heptamethine Cyanines. The Journal of Organic Chemistry. 2020;85(15):9776-90.